Journal of
Applied Remote Sensing

RemoteSensing.SPIEDigitalLibrary.org

Bio-optical model to describe remote sensing signals from a stratified ocean

James H. Churnside

SPIE.

Bio-optical model to describe remote sensing signals from a stratified ocean

James H. Churnside*
NOAA Earth System Research Laboratory, 325 Broadway, Boulder, Colorado 80305, United States

Abstract. We use a bio-optical model of the optical properties of natural seawater to investigate the effects of subsurface chlorophyll layers on passive and active remote sensors. A thin layer of enhanced chlorophyll concentration reduces the remote sensing reflectance in the blue, while having little effect in the green. As a result, the chlorophyll concentration inferred from ocean color instruments will fall between the background concentration and the concentration in the layer, depending on the concentrations and the depth of the layer. For lidar, an iterative inversion algorithm is described that can reproduce the chlorophyll profile within the limits of the model. The model is extended to estimate column-integrated primary productivity, demonstrating that layers can contribute significantly to overall productivity. This contribution also depends on the chlorophyll concentrations and the depth of the layer. Using passive remote sensing alone to estimate primary productivity can lead to significant underestimation in the presence of subsurface plankton layers. Active remote sensing is not affected by this bias. [DOI: 10.1117/1.JRS.9.095989]

Keywords: ocean color; remote sensing; thin-plankton layers; lidar; chlorophyll.

Paper 15262P received Apr. 10, 2015; accepted for publication Oct. 9, 2015; published online Nov. 6, 2015.

1 Introduction

There has been a significant effort to describe passive remote sensor signals for case 1 waters with a semianalytic approach.[1–8] For case 1 waters, the optical properties are assumed to be dominated by pure water contributions and the effects of chlorophyll-containing phytoplankton. In the semianalytic approach, analytic relationships between optical properties of the water are combined with empirical dependencies on chlorophyll concentration. In these studies, the optical properties are assumed to be homogeneous, determined by the value of chlorophyll concentration at the surface.

More recently, the approach has been extended to include case 2 waters,[9–13] generally coastal waters, where the effects of suspended and dissolved materials that are not related to chlorophyll on the optical properties are important. In these investigations, the main motivation was the estimation of chlorophyll concentration from passive remote sensing signals in coastal and estuarine waters.

Other work has focused on deriving additional information from passive remote sensors. One area of investigation has been to obtain information about phytoplankton cell size.[14–17] Another is to identify phytoplankton functional groups.[18–21] A third area is to detect harmful algal blooms.[22–25]

There have been several investigations into the effects of nonuniform vertical distribution of chlorophyll on passive remote sensing signals. Sathyendranath and Platt[26] investigated the effects on the blue-green ratio and found relative errors in excess of 100% in estimates of photic depth and total chlorophyll concentration in the photic zone. Gordon[27] used a Monte-Carlo simulation to test the hypothesis that the reflectance of a stratified ocean is the same as that of a

*Address all correspondence to: James H. Churnside, E-mail: james.h.churnside@noaa.gov

homogeneous ocean with a constant chlorophyll concentration equal to the depth-weighted average of the actual profile, and found that the hypothesis was accurate to within 25% for the cases tested. Stramska and Stramski[28] used a sophisticated radiative transfer model to investigate the effects of a nonuniform depth profile, reporting differences from the uniform profile greater than 70%, with the larger differences produced by lower surface chlorophyll concentrations. Pitarch et al.[29] considered retrieval of the chlorophyll profile using passive remote sensing with some success.

Approximate models of active remote sensor signals have also been developed.[30] The most successful is probably the quasisingle-scattering approximation,[2,31–33] which has been shown to provide good agreement with measured values.[34] This model has recently been used to obtain an expression for the lidar extinction-to-backscatter ratio for lidar inversions[35] that can provide the depth profile of phytoplankton directly.

Roughly, half of the global photosynthesis takes place in the upper ocean, and inversion models have been developed to quantify this production using satellite data.[36–38] These models are generally based on surface chlorophyll concentration from ocean color and sea-surface temperature from thermal radiometers. These estimates do not always agree with *in situ* estimates of productivity, and stratification has been suggested as one possible reason for the discrepancy.[38]

Stratification is important, because phytoplankton are often seen to occur in thin (3 to 5 m or less) layers associated at the pycnocline at the base of the surface mixed layer.[39–41] Most of the observations have been in coastal regions, but thin layers have also been observed in the open ocean.[39] These layers can contain a significant fraction of the total chlorophyll in the water column,[42,43] affecting not only primary production, but also the grazing success of zooplankton and higher-trophic levels.

In this work, we consider a semianalytic bio-optical model to describe passive and active remote sensor signals. To illustrate the effects of stratification, a layer of relatively high-chlorophyll concentration is embedded within a lower-background concentration. The effects of such a layer on primary productivity and on satellite estimates of primary productivity are estimated.

2 Semianalytic Bio-Optical Model

In the semianalytic ocean color model of Gordon et al.,[1]

$$\frac{R}{Q} = 0.0949\frac{b_b}{a+b_b} + 0.0794\left(\frac{b_b}{a+b_b}\right)^2, \tag{1}$$

where R is the irradiance reflectance just below the surface, Q is the ratio of upwelling radiance to upwelling irradiance, b_b is the integral of the scattering coefficient over all possible scattering directions where the scattering angle is greater than 0.5π, and a is the absorption coefficient. This equation is simplified by assuming that the second term is small. Gordon et al.[1] continue with the approximation for the diffuse attenuation coefficient

$$K_d = \frac{1.054(a+b_b)}{\cos(\theta_s)}, \tag{2}$$

where θ_s is the solar zenith angle. They use a nominal solar zenith angle of 25 deg, with the assertion that the resulting error is less than 10% for angles between 0 deg and 34 deg. Rather than take this approach, we will consider a zenith angle of 0 deg; the correction for other zenith angles is straightforward and will be included in the estimates of primary productivity. The result of these approximations is

$$\frac{R}{Q} = 0.10\frac{b_b}{K_d}. \tag{3}$$

For passive remote sensing, we are interested in the remote sensing reflectance, R_{rs}, defined as the ratio of the upwelling radiance to the downwelling irradiance just above the surface. Mobley[44] has shown that R_{rs} can be approximated by $0.54R/Q$, so we have

$$R_{\mathrm{rs}} = 0.054\,\frac{b_b}{K_d}. \tag{4}$$

We expect this approximation to be valid for values less than about 0.01 sr^{-1}. Equation (4) was developed under the assumption that the optical properties of the water are constant with depth. If they are not, it should be possible to estimate the remote sensing reflectance, to the same level of approximation, by the expression

$$R_{\mathrm{rs}} = 0.11 \int_0^{\infty} b_b(z) \exp\left[-2\int_0^{z} K_d(z')\mathrm{d}z'\right]\mathrm{d}z. \tag{5}$$

This equation was developed to have the expected exponential attenuation with depth and to reduce to Eq. (4) when b_b and K_d are constant.

We can relate the remote sensing reflectance to chlorophyll concentration, C, using the model described by Morel and Maritorena.[3] In this model, we have

$$b_b = \frac{1}{2} b_w + 0.416 C^{0.766}\left\{0.002 + 0.01[0.5 - 0.25\log_{10}(C)]\left(\frac{\lambda}{550}\right)^{\upsilon}\right\}, \tag{6}$$

where b_w is the scattering coefficient of pure seawater, λ is the wavelength in nm, and υ is a variable exponent given by

$$\upsilon = 0.5\log_{10}(C) - 0.15 \quad \text{for } 0.02 < C < 2\ \mathrm{mg\,m^{-3}} \quad \upsilon = 0 \quad \text{for } C > 2\ \mathrm{mg\,m^{-3}}. \tag{7}$$

Mobley[44] presents a table of b_w based on the work of Morel.[45] These values can be approximated by

$$b_w = 10^{0.6301 - 9.019\times10^{-3}\lambda + 5.351\times10^{-6}\lambda^2}, \tag{8}$$

with an error in the fit of less than 1% for λ between 350 and 600 nm. This equation neglects the effects of temperature and salinity, and more accurate models are available[46] that include these dependencies. The difference between the Zhang et al.[46] model and Eq. (8) can be significant (e.g., 10% for $\lambda = 550$ nm for a temperature of 20°C and a salinity of 35 PSU).

Morel and Maritorena[3] also present a model for diffuse attenuation given by

$$K_d = K_w + \chi C^e, \tag{9}$$

where K_w is the diffuse attenuation from pure seawater, and χ and e are parameters that vary with wavelength. These three parameters are available in tables.[5] It is occasionally convenient to have approximations to the tabulated values, and we have done this by piecewise polynomial fits. These are

$$\begin{aligned}
K_w &= -81.373033 + 0.98491411\lambda - 0.0047381508\lambda^2 + 1.1334476\times10^{-5}\lambda^3\\
&\quad - 1.3491818\times10^{-8}\lambda^4 + 6.3969794\times10^{-12}\lambda^5, \quad 350 \le \lambda < 515\\
K_w &= 907.42423 - 6.729768\lambda + 0.01871207\lambda^2 - 2.311898\times10^{-5}\lambda^3\\
&\quad + 1.07099\times10^{-8}\lambda^4, \quad 515 \le \lambda < 605,\\
K_w &= -1419.824 + 8.654027\lambda - 0.01970537\lambda^2 + 1.985801\times10^{-5}\lambda^3\\
&\quad - 7.46716\times10^{-9}\lambda^4, \quad 605 \le \lambda < 665,\\
K_w &= -1373.958 + 6.150477\lambda - 9.177511\times10^{-3}\lambda^2 + 4.56626263\times10^{-6}\lambda^3,\\
&\quad 665 \le \lambda \le 700,
\end{aligned} \tag{10}$$

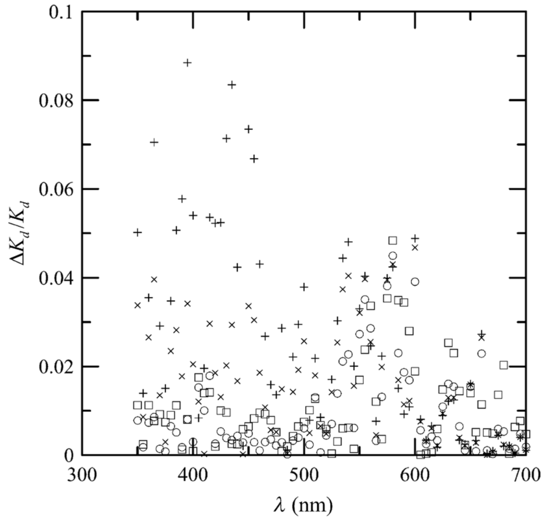

Fig. 1 Relative error in K_d estimated from Eqs. (10)–(12), relative to that using the tabulated values for chlorophyll concentrations of $C = 0.01$ (+), 0.1 (×), 1 (○), and 10 (□) $mg\,m^{-3}$.

$$\begin{aligned}
\chi &= -11.5717 + 0.0982478\lambda - 2.72055\times10^{-4}\lambda^2 + 2.48741\times10^{-7}\lambda^3, \quad 350 \le \lambda < 415,\\
\chi &= -6.22839 + 0.05027291\lambda - 1.440342\times10^{-4}\lambda^2 + 1.769267\times10^{-7}\lambda^3\\
&\quad - 7.919928\times10^{-11}\lambda^4, \quad 415 \le \lambda < 675,\\
\chi &= -1.5063 + 5.44393\times10^{-3}\lambda - 4.64286\times10^{-6}\lambda^2, \quad 675 \le \lambda \le 700,
\end{aligned} \tag{11}$$

$$\begin{aligned}
e &= 4.06652 - 0.0151677\lambda + 1.65361\times10^{-5}\lambda^2, \quad 350 \le \lambda < 400,\\
e &= 1.26402 - 7.31889\times10^{-3}\lambda + 2.27559\times10^{-5}\lambda^2 - 2.08551\times10^{-8}\lambda^3, \quad 400 \le \lambda < 580,\\
e &= 0.799443 - 1.40758\times10^{-3}\lambda + 1.86375\times10^{-6}\lambda^2, \quad 400 \le \lambda < 675,\\
e &= -12.6864 + 0.0429771\lambda - 3.42857\times10^{-5}\lambda^2, \quad 675 \le \lambda \le 700.
\end{aligned} \tag{12}$$

The number of segments, the degree of the polynomials, and the number of significant digits for the coefficients have been selected so that the errors in chlorophyll concentration produced by this approximation are 10% or less. The resulting error in the estimate of K_d is plotted in Fig. 1. The errors are all less than 5%, except for very low-chlorophyll concentration near the minimum absorption. Here, K_d is very small and the errors are dominated by those in our estimate of K_w. The root-mean-square error for all values is 2.2%.

Several examples of remote sensing spectra (Fig. 2) confirm that the values are generally below 0.01 sr^{-1}, and the second term in Eq. (1) can be neglected. These examples also show that the piecewise polynomial fit reproduces the remote sensing reflectance spectra obtained from the tabulated parameters.

For active remote sensing, similar expressions can be used. We will restrict ourselves to a broad-beam, unpolarized lidar for which the received signal can be written as[30,33]

$$s(z) = A\beta(\pi, z)\exp\left[-2\int_0^z K_d(z')\mathrm{d}z'\right], \tag{13}$$

where A is a calibration constant and $\beta(\pi)$ is the volume scattering coefficient at a scattering angle of π radians. The volume scattering function is the product of the scattering phase function and the scattering coefficient. At the scattering angle of interest, this is the sum of water and particulate contributions

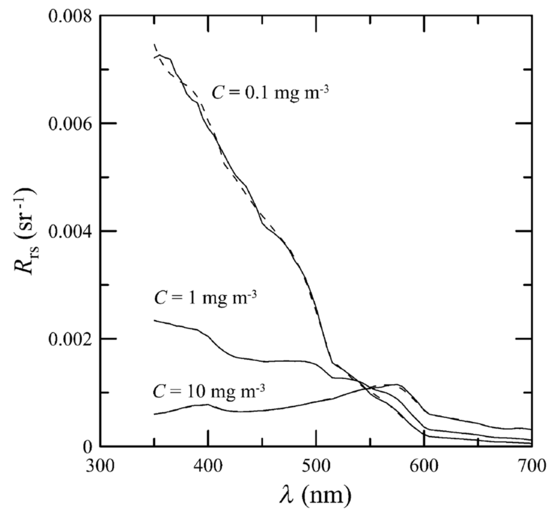

Fig. 2 Remote sensing reflectance, R_{rs}, versus wavelength, λ, for the tabulated parameters (solid lines) and the piecewise polynomial fit (dashed lines) for several values of chlorophyll concentration C.

$$\beta(\pi) = 0.114 b_w + 0.151\left(b_b - \frac{1}{2} b_w\right), \tag{14}$$

where 0.114 is the phase function of pure seawater[44] and 0.151 is a linear extrapolation of the model of Sullivan and Twardowski[47] to the scattering angle of π steradians. This can be evaluated using Eqs. (6) and (8).

There are two reasons for preferring a broad beam. The primary one is that it provides the minimum attenuation possible at a given wavelength,[30,32] which results in the maximum penetration depth. This is a consequence of the distribution of particulate scattering in the ocean, which is dominated by scattering at small angles. Most scattered light will remain within a broad beam, and not contribute to attenuation. For a narrow beam, this light will be scattered outside of the beam, and does contribute to overall attenuation. A secondary advantage is that a broader beam is less likely to pose a laser-exposure risk.[48]

The only reason to consider unpolarized lidar is that we do not currently have a good model for polarization characteristics. This is an area that deserves more attention, since layers are much more detectable by polarization lidar.[34,39,49,50]

3 Estimating Chlorophyll

The operational chlorophyll algorithms have the form

$$\log(C) = \sum_{n=0}^{4} a_i \left\{ \log\left[\frac{R_{rs}(\lambda_{\text{blue}})}{R_{rs}(\lambda_{\text{green}})}\right] \right\}^n, \tag{15}$$

where the blue and green wavelengths and the coefficients depend on the particular instrument. To illustrate, we will use a modified version of the OC3M algorithm[51] for the moderate resolution imaging spectroradiometer. The OC3M algorithm is an empirical fit to a large dataset,[52] and Eq. (15) can be written as

$$y = 0.2424 - 2.7423x + 1.8017x^2 + 0.0015x^3 - 1.2280x^4, \tag{16}$$

where the blue wavelength is 443 or 488 nm, depending on which has the larger value of R_{rs}, and the green wavelength is 547 nm. One can check the self-consistency of the model by using chlorophyll concentration to calculate remote sensing reflectances and then applying the OC3M algorithm on these reflectances to estimate chlorophyll concentration. The result (Fig. 3) shows a

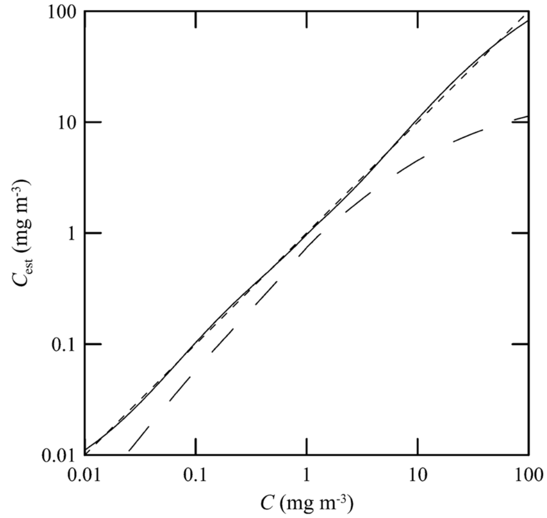

Fig. 3 Estimated chlorophyll concentration, C_{est}, as a function of the concentration used in the bio-optical model, C, for the OC3M algorithm (long dashes) and the modified algorithm of Eq. (17) (solid line). Short dashes provide the desired one-to-one relationship.

bias in estimated chlorophyll concentration, especially at high chlorophyll concentrations, where the assumptions of the model may not be valid.

The OC3M algorithm can be modified to fit our bio-optical model, with the result

$$y = 0.3925 - 3.4848x + 5.7269x^2 - 7.8295x^3 + 3.1113x^4. \tag{17}$$

This provides a self-consistent model that can be used to investigate the effects of layers on inferred values of chlorophyll.

To estimate C from 532 nm lidar data, we will use the modified lidar extinction-to-backscatter ratio[35]

$$S_{\text{lidar}} = \frac{K_d - K_w}{\beta(\pi) - 0.114 b_w}. \tag{18}$$

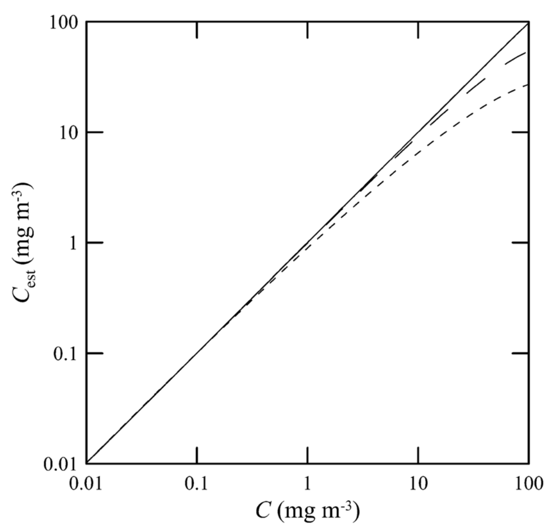

Fig. 4 Estimated chlorophyll concentration, C_{est}, as a function of the concentration used in the bio-optical model, C, for the iterative lidar inversion. The short dashed line is the first estimate, the long dashed line is the second estimate, and the solid line is the 10th estimate, which is indistinguishable from the actual value.

If S_{lidar} is known, the chlorophyll concentration can be estimated from Eqs. (9) and (18)

$$C_{\text{est}} = \left(\frac{K_d - K_w}{\chi}\right)^{\frac{1}{e}} = \{[21.1\beta(\pi) - 4.09 \times 10^{-3}]S\}^{1.5}, \tag{19}$$

where numerical values for $\lambda = 532$ nm were used in the second step. The attenuation coefficient, needed to find β below the surface, can be estimated from Eq. (18) by

$$K_{d\text{est}} = S[\beta(\pi) - 1.94 \times 10^{-4}] + 0.0452. \tag{20}$$

The actual estimate of C can be found iteratively. We begin with a value of $S = 100$ and calculate C_{est}. That value is used to calculate a new estimate for S from Eq. (19), which is used to calculate a new C_{est}. The first estimate is close to the actual value for small concentrations (Fig. 4). By the 10th iteration, the estimate is within 2.5% of the actual value, even for very high values of C. To obtain depth profiles, one starts at the surface sample and works progressively deeper, using the estimated attenuation profile to obtain the actual value of β from the measured signal at each depth.

4 Primary Productivity

We can investigate the effects of thin layers on primary productivity using a model based on chlorophyll concentration.[36,37] We will use the vertically generalized production model, which takes the form

$$\text{PP} = P_{\text{opt}}^{B} D \int_0^{Z_{\text{eu}}} \frac{\left\{1 - \exp\left[-\frac{E(z)}{E_{\max}}\right]\right\} \exp[-\beta_p E(z)]}{\left\{1 - \exp\left[-\frac{E_{\text{opt}}}{E_{\max}}\right]\right\} \exp[-\beta_p E_{\text{opt}}]} C(z)\mathrm{d}z, \tag{21}$$

where PP is the daily primary productivity in the euphotic zone ($\text{mg C m}^{-2}\,\text{day}^{-1}$), P_{opt}^{B} is the maximum carbon fixation rate within the water column, [$\text{mg C (mg chl)}^{-1}\,\text{h}^{-1}$], D is the photoperiod (hour), Z_{eu} is the depth of the euphotic zone, E is the photosynthetically active radiation (PAR; mol quanta m^{-2}), $E_{\max}$ is the daily PAR at the inflection point between light limitation and light saturation in the absence of photoinhibition, β_p is a photoinhibition parameter, E_{opt} is the daily PAR at the depth of $PC_{\max}$, and C is the chlorophyll concentration (mg m^{-3}).

$$P_{\text{opt}}^{B} = 1.2956 + 0.2749T + 0.0617T^2 - 0.0205T^3 + 2.462 \times 10^{-3}T^4 - 1.348 \times 10^{-4}T^5 + 3.4132 \times 10^{-6}T^6 - 3.27 \times 10^{-8}T^7, \tag{22}$$

where T is the water temperature in °C.

$$E_{\max} = 0.3195E_0, \tag{23}$$

where E_0 is the daily PAR at the surface in mol m^{-2}.

$$E_{\text{opt}} = E_0 \exp(+0.00137 - 0.075E_0 + 0.00171E_0^2 - 1.84 \times 10^{-5}E_0^3 + 7.56 \times 10^{-8}E_0^4), \tag{24}$$

$$\beta_p = 0.1 \quad \text{for } E_0 \leq 3\ \text{mol m}^{-2} = -0.0203\ \ln(E_0) + 0.124 \quad \text{for } E_0 > 3\ \text{mol m}^{-2}. \tag{25}$$

Surface PAR was estimated using MODTRAN4[53] with no clouds and the appropriate standard aerosol model. For the example of year day 180 and latitude of 45°N, this would be the midlatitude summer model. Values were integrated over the 400 to 700 nm PAR band and over daylight hours. Subsurface values were estimated using an assumed attenuation coefficient of[6]

$$K_{\mathrm{PAR}} = 0.121C^{0.428}. \tag{26}$$

Behrenfeld and Falkowski[37] concluded that replacing the chlorophyll profile by the surface concentration produces acceptable results. In this case, satellite estimates of surface chlorophyll concentration, aerosol optical depth, and sea-surface temperature can provide global estimates of oceanic primary productivity using the approximate equation

$$\mathrm{PP} = 0.66125 P_{\mathrm{opt}}^{B} D\, C(0) Z_{\mathrm{eu}} \frac{E(0)}{E(0) + 4.1}, \tag{27}$$

where Z_{eu} is estimated from[54]

$$Z_{\mathrm{eu}} = 568.2 C_{\mathrm{tot}}^{-0.746} \quad \text{for } Z_{\mathrm{eu}} < 102\ \mathrm{m} = 200 C_{\mathrm{tot}}^{-0.293} \quad \text{for } Z_{\mathrm{eu}} > 102\ \mathrm{m}, \tag{28}$$

with

$$C_{\mathrm{tot}} = 38.0 C(0)^{0.425} \quad \text{for } C(0) < 1\ \mathrm{mg\,m^{-3}} = 40.2 C(0)^{0.507} \quad \text{for } C(0) < 1\ \mathrm{mg\,m^{-3}}. \tag{29}$$

This and similar models allow global estimation of primary productivity from satellite data, although there are differences between models and between modeled and measured productivity.[38]

5 Stratified Water Example

To illustrate the effects of stratification, we will consider the case of a layer of water with $C = C_l$ within region with a background level, $C = C_b$. The top of the layer is at depth z_0 and the bottom at z_1 (Fig. 5). For this geometry, it is straightforward to perform the integrations in Eq. (5), with the result

$$R_{\mathrm{rs}} = R_b\{1 - \exp(-2K_b z_0)[1 - \exp(-2K_l L)]\} + R_l\{\exp(-2K_b z_0)[1 - \exp(-2K_l L)]\}, \tag{30}$$

where L is the layer thickness, $L = z_1 - z_2$, K_b and K_l refer to diffuse attenuation estimated using C_b and C_l, and R_b and R_l refer to remote sensing reflectance calculated with Eq. (4) using C_b and C_l. This result was presented in a slightly more general form by Zaneveld and Pegau.[55]

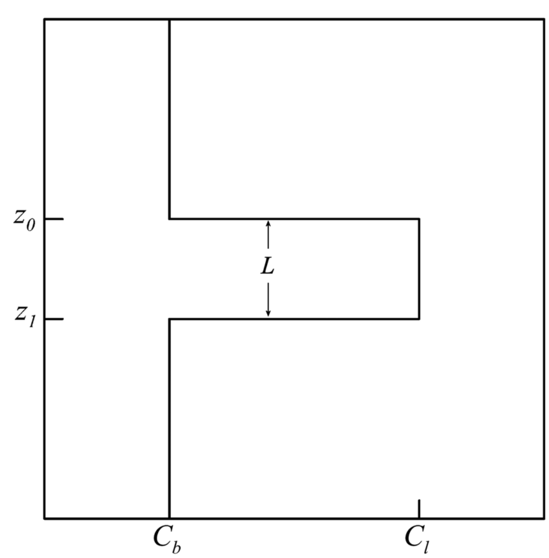

Fig. 5 Schematic of layer used for calculations. A layer with chlorophyll concentration C_l and thickness L is located with its top at a depth z_0. Background chlorophyll concentration above and below the layer is C_b.

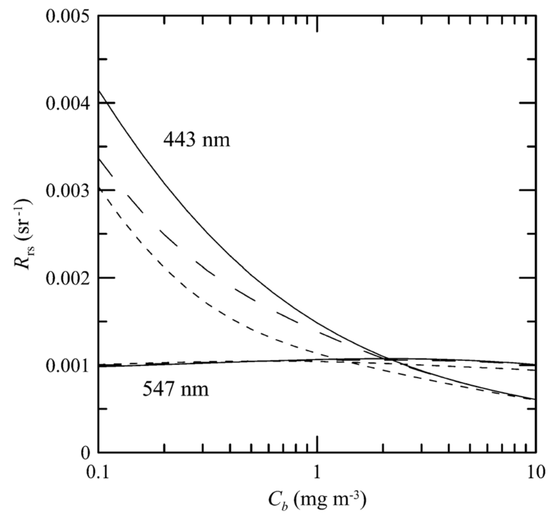

Fig. 6 Remote sensing reflectance, R_{rs}, as a function of background chlorophyll concentration, C_b, for wavelengths of 443 and 547 nm. For each wavelength, curves are plotted for no layer (solid line) and 3-m thick layers at depths of 5 m (short-dashed line) and 10 m (long-dashed line).

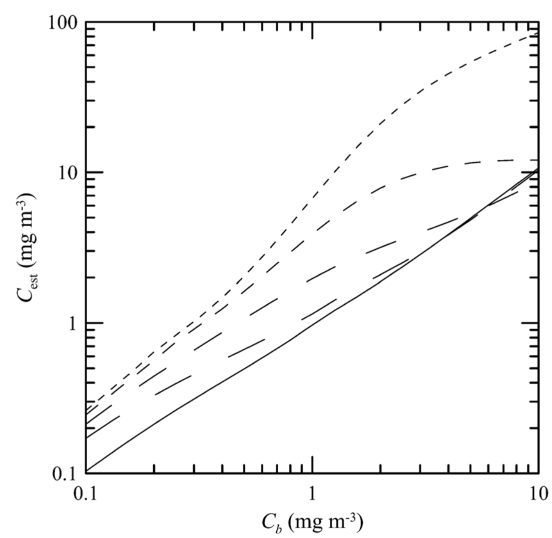

Fig. 7 Estimated chlorophyll concentration, C_{est}, as a function of background concentration, C_b, for the case of no layer (solid line), a 3-m layer at the surface (short dashed line), and at depths of 2.5, 5, and 10 m (dashed lines with increasing dash length).

As expected, Eq. (30) reduces to $R_{\mathrm{rs}} = R_b$ for $C_l = C_b$, for $L = 0$, or for $z_0 = \infty$. Similarly, it reduces to $R_{\mathrm{rs}} = R_l$ for $z_0 = 0$ or for $L = \infty$.

We considered the example of two wavelengths used in the OC3M algorithm, 443 nm in the blue and 547 nm in the green, and a 3-m thick layer whose chlorophyll concentration was 10 times the background concentration. The factor-of-ten enhancement is consistent with reported values that include a range of 4-55 in Monterey Bay, California[56] and a median value of 12 in open water in the Arctic Ocean.[57] A minimum value of three was used as a criterion for the existence of a layer in East Sound, Washington,[40] suggesting typical values were much higher. However, other measurements in Monterey Bay have produced average values of about three,[42,58] suggesting that there is a high degree of variability. Figure 6 presents the results for layers at depths (to the center of the layer) of 5 and 10 m, along with the results without a layer. The effect of the layer is most pronounced at the blue wavelength, especially at the shallower depth and at lower values of chlorophyll concentration. The effect is small at the

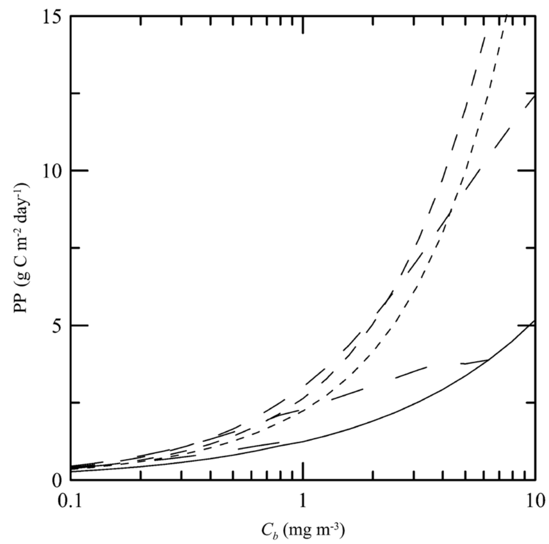

Fig. 8 Calculated column-integrated primary productivity, PP, as a function of background chlorophyll concentration, C_b, for the case of no layer (solid line), and 3 m layers at depths of 2.5, 5, 10, 20, and 40 m (dashed lines with increasing dash length).

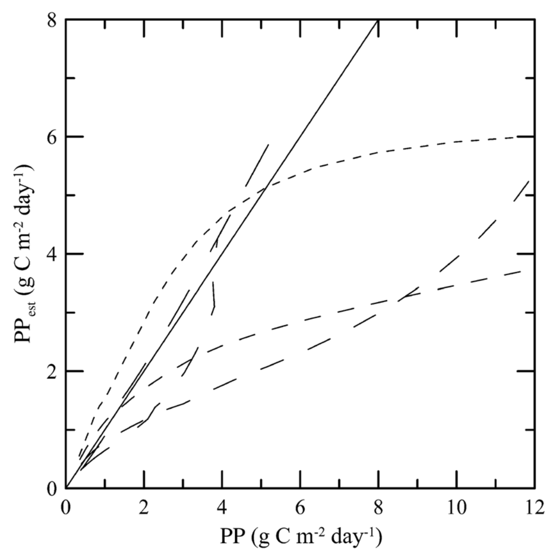

Fig. 9 Estimated column-integrated primary productivity, PP_{est}, as a function of calculated productivity, PP, for 3 m thick layers at depths of 2.5, 5, 10, 20, and 40 m (dashed lines with increasing dash length). Solid line is $PP_{est} = PP$.

green wavelength, where R_{rs} is nearly constant over a wide range of chlorophyll concentrations. The spectra of Fig. 2 illustrate that this lack of sensitivity is a consequence of the selection of 547 nm as the green wavelength.

The shift in remote sensing reflectance will affect the inferred chlorophyll concentration. Using the same conditions of a 3-m thick layer whose concentration is 10 times the background concentration, we investigated the effects of layer depth (Fig. 7). At low-background concentrations, the concentration inferred from remote sensing reflectance is generally higher than the background concentration for shallow layers. At higher background concentrations, the layer has much less of an effect unless it is right at the surface.

To illustrate the effects on primary productivity, we will consider a midlatitude (45°N), midsummer (year day 180) example (Fig. 8). As the background chlorophyll concentration increases, deeper layers see less light and contribute less to the total productivity. For a layer at 40 m, the contribution from the layer goes to zero when $C_B = 1\ \mathrm{mg\,m^{-3}}$. For a layer at 20 m, this happens at $C_B = 6\ \mathrm{mg\,m^{-3}}$. The maximum productivity for this example generally occurs for a layer at 5 to 10 m deep.

The comparison of calculated productivity with that estimated from satellite measurements (Fig. 9) shows that significant errors can occur when thin layers are present. For layers at depths of 5 to 10 m, productivity is underestimated by more than a factor of two. For the deepest layer, the satellite estimate is about 8% greater than the calculated value. This is a result of the approximations inherent in Eq. (24) rather than an effect of the layer.

6 Conclusions

The remote-sensing reflectance of the ocean will be affected by the presence of thin layers of enhanced chlorophyll concentration. For case 1 waters, a bio-optical model was used to demonstrate that this effect depends on the background chlorophyll concentration, enhancement in the layer, depth of the layer, and optical wavelength. Because of the wavelength dependence, estimates of chlorophyll concentration-based ratios of remote sensing reflectance at different wavelengths will also be affected. This effect leads to estimates of primary productivity that are too low when ocean color alone is used.

Thin layers at 5–10 m depths produce the worst estimates of chlorophyll concentration and primary productivity. This is significant for productivity at midlatitudes because the seasonal thermocline that would support layers at these depths is typically shallow in spring and summer when productivity is greatest. In fact, thin layers within this depth range are common in Monterey Bay, California,[59] East Sound, Washington,[40] West Sound, Washington,[49] and elsewhere.[39] Deeper layers are also common, and the total column-integrated chlorophyll concentration will be underestimated where these occur. These layers receive less sunlight, however, and their contribution to total primary productivity is small.

The same bio-optical model can be used to describe the signal from a profiling lidar. With the application of a previously developed relationship between backscatter and attenuation and a new inversion technique, the lidar signal reproduces the profile of chlorophyll concentration, including the characteristics of the layer. As a result, estimates of primary productivity obtained from lidar do not exhibit the same bias inherent in those obtained from ocean color. With this model, future work will concentrate on combining active and passive sensors to improve estimates of chlorophyll concentration and primary productivity using the spectral information from passive sensors and the profile information from active sensors.

References

1. H. R. Gordon et al., "A semianalytic radiance model of ocean color," *J. Geophys. Res. Atmos.* **93**(D9), 10909–10924 (1988).
2. H. R. Gordon, "Simple calculation of the diffuse reflectance of the ocean," *Appl. Opt.* **12**(12), 2803–2804 (1973).
3. A. Morel and S. Maritorena, "Bio-optical properties of oceanic waters: a reappraisal," *J. Geophys. Res. Oceans* **106**(C4), 7163–7180 (2001).
4. A. Bricaud et al., "Variations of light absorption by suspended particles with chlorophyll a concentration in oceanic (case 1) waters: analysis and implications for bio-optical models," *J. Geophys. Res. Oceans* **103**(C13), 31033–31044 (1998).
5. H. Loisel and A. Morel, "Light scattering and chlorophyll concentration in case 1 waters: a reexamination," *Limnol. Oceanogr.* **43**(5), 847–858 (1998).
6. A. Morel, "Optical modeling of the upper ocean in relation to its biogenous matter content (case I waters)," *J. Geophys. Res. Oceans* **93**(C9), 10749–10768 (1988).
7. H. R. Gordon and A. Morel, "Remote assessment of ocean color for interpretation of satellite visible imagery, a review," in *Lecture Notes on Coastal and Estuarine Studies*, p. 114, Springer Verlag, New York (1983).
8. A. Morel, D. Antoine, and B. Gentili, "Bidirectional reflectance of oceanic waters: accounting for Raman emission and varying particle scattering phase function," *Appl. Opt.* **41**(30), 6289–6306 (2002).

9. Z. Lee, K. L. Carder, and R. A. Arnone, "Deriving inherent optical properties from water color: A multiband quasi-analytical algorithm for optically deep waters," *Appl. Opt.* **41**(27), 5755–5772 (2002).
10. J. Huang et al., "Validation of semi-analytical inversion models for inherent optical properties from ocean color in coastal Yellow Sea and East China Sea," *J. Oceanogr.* **69**(6), 713–725 (2013).
11. L. Cheng Feng et al., "Validation of a quasi-analytical algorithm for highly turbid eutrophic water of Meiliang Bay in Taihu Lake, China," *IEEE Trans. Geosci. Remote Sens.* **47**(8), 2492–2500 (2009).
12. P. Shanmugam et al., "An evaluation of inversion models for retrieval of inherent optical properties from ocean color in coastal and open sea waters around Korea," *J. Oceanogr.* **66**(6), 815–830 (2010).
13. J. Chen, X. Zhang, and W. Quan, "Retrieval chlorophyll-a concentration from coastal waters: three-band semi-analytical algorithms comparison and development," *Opt. Express* **21**(7), 9024–9042 (2013).
14. V. Brotas et al., "Deriving phytoplankton size classes from satellite data: validation along a trophic gradient in the eastern Atlantic Ocean," *Remote Sens. Environ.* **134**, 66–77 (2013).
15. R. J. Brewin et al., "The influence of the Indian Ocean dipole on interannual variations in phytoplankton size structure as revealed by earth observation," *Deep Sea Res. II* **77**, 117–127 (2012).
16. R. J. Brewin et al., "An intercomparison of bio-optical techniques for detecting dominant phytoplankton size class from satellite remote sensing," *Remote Sens. Environ.* **115**(2), 325–339 (2011).
17. R. J. Brewin et al., "A three-component model of phytoplankton size class for the Atlantic Ocean," *Ecol. Model.* **221**(11), 1472–1483 (2010).
18. P. J. Werdell, C. S. Roesler, and J. I. Goes, "Discrimination of phytoplankton functional groups using an ocean reflectance inversion model," *Appl. Opt.* **53**(22), 4833–4849 (2014).
19. Z. B. Mustapha et al., "Automatic classification of water-leaving radiance anomalies from global SeaWiFS imagery: application to the detection of phytoplankton groups in open ocean waters," *Remote Sens. Environ.* **146**, 97–112 (2013).
20. S. Alvain, H. Loisel, and D. Dessailly, "Theoretical analysis of ocean color radiances anomalies and implications for phytoplankton groups detection in case 1 waters," *Opt. Express* **20**(2), 1070–1083 (2012).
21. S. Alvain et al., "Use of global satellite observations to collect information in marine ecology," in *Sensors for Ecology*, J.-F. L. Galliard, J.-M. Guarini, and F. Gaill, Eds., pp. 227–242, CNRS, Paris (2012).
22. T. T. Wynne et al., "Detecting Karenia brevis blooms and algal resuspension in the western Gulf of Mexico with satellite ocean color imagery," *Harmful Algae* **4**(6), 992–1003 (2005).
23. V. Klemas, "Remote sensing of algal blooms: an overview with case studies," *J. Coast. Res.* **28**(1A), 34–43 (2012).
24. T. Kutser, "Passive optical remote sensing of cyanobacteria and other intense phytoplankton blooms in coastal and inland waters," *Int. J. Remote Sens.* **30**(17), 4401–4425 (2009).
25. L. Shen et al., "Oceanography of Skeletonema costatum harmful algal blooms in the East China Sea using MODIS and QuickSCAT satellite data," *J. Appl. Remote Sens.* **6**(1), 063529 (2012).
26. S. Sathyendranath and T. Platt, "Remote sensing of ocean chlorophyll: consequence of non-uniform pigment profile," *Appl. Opt.* **28**(3), 490–495 (1989).
27. H. R. Gordon, "Diffuse reflectance of the ocean: influence of nonuniform phytoplankton pigment profile," *Appl. Opt.* **31**(12), 2116–2129 (1992).
28. M. Stramska and D. Stramski, "Effects of a nonuniform vertical profile of chlorophyll concentration on remote-sensing reflectance of the ocean," *Appl. Opt.* **44**(9), 1735–1747 (2005).
29. J. Pitarch et al., "Retrieval of vertical particle concentration profiles by optical remote sensing: a model study," *Opt. Express* **22**(S3), A947–A959 (2014).
30. J. H. Churnside, "Review of profiling oceanographic lidar," *Opt. Eng.* **53**(5), 051405 (2014).

31. L. S. Dolin and V. A. Saveliev, "Backscattering signal characteristics at pulse narrow beam illumination of a turbid medium," *Izv. Akad. Nauk Fiz. Atmos. Okeana* **7**, 505–510 (1971).
32. H. R. Gordon, "Interpretation of airborne oceanic lidar: effects of multiple scattering," *Appl. Opt.* **21**, 2996–3001 (1982).
33. J. H. Churnside, "Polarization effects on oceanographic lidar," *Opt. Express* **16**(2), 1196–1207 (2008).
34. J. H. Lee et al., "Oceanographic lidar profiles compared with estimates from in situ optical measurements," *Appl. Opt.* **52**(4), 786–794 (2013).
35. J. H. Churnside, J. M. Sullivan, and M. S. Twardowski, "Lidar extinction-to-backscatter ratio of the ocean," *Opt. Express* **22**(15), 18698–18706 (2014).
36. M. J. Behrenfeld and P. G. Falkowski, "A consumer's guide to phytoplankton primary productivity," *Limnol. Oceanogr.* **42**(7), 1479–1491 (1997).
37. M. J. Behrenfeld and P. G. Falkowski, "Photosynthetic rates derived from satellite-based chlorophyll concentration," *Limnol. Oceanogr.* **42**(1), 1–20 (1997).
38. Z. Lee et al., "Estimating oceanic primary productivity from ocean color remote sensing: a strategic assessment," *J. Mar. Syst.* **149**, 50–59 (2015).
39. J. H. Churnside and P. L. Donaghay, "Thin scattering layers observed by airborne lidar," *ICES J. Mar. Sci.* **66**(4), 778–789 (2009).
40. M. M. Dekshenieks et al., "Temporal and spatial occurrence of thin phytoplankton layers in relation to physical processes," *Mar. Ecol. Prog. Ser.* **223**, 61–71 (2001).
41. W. M. Durham and R. Stocker, "Thin phytoplankton layers: characteristics, mechanisms, and consequences," *Annu. Rev. Mar. Sci.* **4**(1), 177–207 (2011).
42. J. M. Sullivan, P. L. Donaghay, and J. E. B. Rines, "Coastal thin layer dynamics: Consequences to biology and optics," *Cont. Shelf Res.* **30**(1), 50–65 (2010).
43. J. M. Sullivan et al., "Layered organization in the coastal ocean: An introduction to planktonic thin layers and the LOCO project," *Cont. Shelf Res.* **30**(1), 1 (2010).
44. C. D. Mobley, *Light and Water: Radiative Transfer in Natural Waters*, Academic Press, San Diego (1994).
45. A. Morel, "Optical properties of pure water and pure sea water," in *Optical Aspects of Oceanography*, N. G. Jerlov and E. S. Nielsen, Eds., pp. 1–24, Academic Press, San Diego (1974).
46. X. Zhang, L. Hu, and M.-X. He, "Scattering by pure seawater: effect of salinity," *Opt. Express* **17**(7), 5698–5710 (2009).
47. J. M. Sullivan and M. S. Twardowski, "Angular shape of the oceanic particulate volume scattering function in the backward direction," *Appl. Opt.* **48**(35), 6811–6819 (2009).
48. H. M. Zorn, J. H. Churnside, and C. W. Oliver, "Laser safety thresholds for cetaceans and pinnipeds," *Mar. Mamm. Sci.* **16**(1), 186–200 (2000).
49. J. H. Churnside et al., "Airborne lidar detection and characterization of internal waves in a shallow fjord," *J. Appl. Remote Sens.* **6**(1), 063611 (2012).
50. J. H. Churnside and L. A. Ostrovsky, "Lidar observation of a strongly nonlinear internal wave train in the Gulf of Alaska," *Int. J. Remote Sens.* **26**(1), 167–177 (2005).
51. NASA Ocean Biology Processing Group, "Algorithm descriptions, chlorophyll a (chlor_a)," http://oceancolor.gsfc.nasa.gov/cms/atbd/chlor_a (4 May 2015).
52. P. J. Werdell and S. W. Bailey, "An improved in-situ bio-optical data set for ocean color algorithm development and satellite data product validation," *Remote Sens. Environ.* **98**(1), 122–140 (2005).
53. G. P. Anderson et al., "MODTRAN4: Radiative transfer modeling for remote sensing," *Proc. SPIE* **4049**, 176–183 (2000).
54. A. Morel and J. F. Berthon, "Surface pigments, algal biomass profiles, and potential production of the euphotic layer: Relationships reinvestigated in view of remote-sensing applications," *Limnol. Oceanogr.* **34**(8), 1545–1562 (1989).
55. J. R. V. Zaneveld and W. S. Pegau, "A model for the reflectance of thin layers, fronts, and internal waves and its inversion," *Oceanography* **11**(1), 44–47 (1998).
56. J. P. Ryan et al., "Phytoplankton thin layers caused by shear infrontal zones of a coastal upwelling system," *Mar. Ecol. Prog. Ser.* **354**, 21–34 (2008).

57. J. H. Churnside and R. Marchbanks, "Sub-surface plankton layers in the Arctic Ocean," *Geophys. Res. Lett.* **42**, 4896–4902 (2015).
58. J. P. Ryan, M. A. McManus, and J. M. Sullivan, "Interacting physical, chemical and biological forcing of phytoplankton thin-layer variability in Monterey Bay, California," *Cont. Shelf Res.* **30**(1), 7–16 (2010).
59. O. Cheriton et al., "Physical and biological controls on the maintenance and dissipation of a thin phytoplankton layer," *Mar. Ecol. Prog. Ser.* **378**, 55–69 (2009).

James H. Churnside received his PhD from the Oregon Graduate Center in 1978, after which he joined the technical staff of the Aerospace Corporation. In 1985, he joined the NOAA Environmental Technology Laboratory, now the Earth System Research Laboratory, where he is currently developing airborne instrumentation for marine ecosystem studies. He has published 96 articles in refereed journals and holds four patents. He is a fellow of OSA and SPIE.